Energy spectrums through Lattice QCD

Sarah Skinner

Advisor: Dr. Colin Morningstar

May 2022

1 Introduction and Motivation (∼1)

Since the dawn of particle physics, experiments have shown that particles have a much more complicated nature than we could ever hope for. Though all detectable particles can be organized in three simple categories—hadrons, leptons, and bosons—describing the makeup and interactions of these particles has proven to be quite challenging. The Standard Model describes all of the most basic particles and the forces mediating them. The fundamental forces are the electroweak force, strong force, and gravity, and though the gravity is incredibly important, particles are usually held together by electroweak and strong interactions. In particular, hadrons, particles made up of quarks (up, down, strange...), are held together by the strong force. In our research, we study the strong force alone.

Quantum chromodynamics (QCD) is the description of strong force interactions using quark and gluon fields. The strong force is characterized by the color charge symmetry $SU(3)$ in the quark fields and mediating non-Abelian gluon fields. The non-Abelian nature of the theory and inclusion of the color charge makes QCD much more difficult to calculate than Quantum Electrodynamics (QED). For high energy interactions ($q^2 \approx m_Z^2 \approx 8320\text{GeV}^2$)[1] [1], QCD contribution to the interactions has a weak coupling of the quark to the gluon and can be calculated perturbatively in an effective field theory (EFT) for that energy regime [2] [3]. For low energy interactions ($q^2 \approx m_\pi^2 \approx 0.018\text{GeV}^2$) [1], EFTs based on chiral symmetry breaking (chiral EFT) has shown promise [4]. In the ($q^2 \approx 1\text{GeV}^2$) regime, the coupling is too strong for a perturbative expansion and the the energy range is well outside the chiral EFT limit which relies on small contributions from excited states. Lattice QCD has been an emerging field that does not have such issues with the coupling, though it has had many challenges in itself. With advanced numerical techniques as well as increased computing power, energy spectrums and masses can be computed from the original QCD Lagrangian rather than an EFT. Due to the complexity and intensity of calculations required, Lattice QCD has only begun to calculate basic observables, but in combination with EFTs, more theoretical results with increased precision and accuracy can be obtained.

In an upcoming experiment, DUNE, this instance is just the case: there are needed theoretical calculations out of reach from EFTs. Neutrinos only interact via the weak force and gravity, because the weak force has such short-range interactions, neutrinos are very unlikely to interact with matter. DUNE plans to detect them using massive Argon detectors, which have had success in recent experiments. Argon is chosen due to its stable atomic configuration, but when high energy neutrinos interact with the nucleons or electrons, a plethora of interactions can occur. In order to learn more about the neutrinos every possible interaction must be considered and accounted for in the cross-sections. A large number of interactions, including the $\Delta(1232MeV)$ resonance, are in the intermediate energy range described above and will require the use of Lattice QCD rather than the traditional EFT's. [5] [6]

[1] q^2 is the transfer four-momentum squared in natural units ($\hbar = c = 1$)

2 Methods and Approach (∼1)

Lattice QCD uses path integral quantization and Monte Carlo to describe the natural quantum behavior of particles. To gain a full scope of this, rather than diving right into fermion and gluon fields, I will first retrieve the energy spectrum from the one-dimensional (1D) simple harmonic oscillator (SHO) using the same techniques as in Lattice QCD [7]. To begin this process, we need to know the Lagrangian of the theory. The Lagrangian that describes the dynamics of a 1D SHO with mass, m, is

$$L = \frac{1}{2}m\dot{x}^2 - \frac{1}{2}m\omega^2 x^2 \tag{1}$$

where x is the position of the mass and $\dot{x} = \frac{dx}{dt}$. The action is the integration of the Lagrangian from time t_a to t_b:

$$S = \int_{t_a}^{t_b} dt\ L(x, \dot{x}). \tag{2}$$

Due to the nature of quantum mechanics, for a well-defined $x(t_a)$ there is not a well-defined $x(t_b)$, but there are well defined probabilities $\phi(x,t)$ (as defined by the Shrödinger equation in the nonrelativistic limit) of the max existing at x at time t. But we are more interested in the transition amplitude, which describes the probability of a particle starting at position (t_a, x_a) and ending up at position (t_b, x_b):

$$Z(b,a) = \langle x_b(t_b)|x_a(t_a)\rangle = \lim_{N\to\infty}\int_{-\infty}^{\infty}\frac{dx_1}{A}\frac{dx_2}{A}...\frac{dx_{N-1}}{A}\exp(\frac{iS}{\hbar}) = \int_a^b \mathcal{D}x\ e^{iS/\hbar}, \tag{3}$$

where dimension of t is discretized using the relation $N\varepsilon \equiv t_b - t_a$ as described in Figure 1 and A is the normalization constant tuned to the Shrödinger equation. At this point, we have discretized the time domain, but continuum results can be obtained when $N \to \infty$ and $\varepsilon \to 0$. For ease of the Monte Carlo calculations and future spectrum calculations, we perform a Wick rotation of the time domain, $t \to -i\tau$. This results in a transition amplitude of

$$Z(b,a) = \int_a^b \mathcal{D}x\ e^{-S/\hbar}. \tag{4}$$

Written this way, $Z(a,b)$ is integral over all paths weighted by the value $\exp(-S/\hbar)$. By definition of classical motion, the heaviest weight is determined by the classical path.

To get an understanding how each path contributes to $Z(a,b)$, several paths are mapped out in Figure 2. Monte Carlo integration includes randomly choosing paths that contribute to $Z(a,b)$, as seen in figure 2b. Most randomly determined paths without any filtering have a low probability and therefore a small contribution to $Z(a,b)$. To map out the high probability paths and achieve a better picture of the quantum fluctuations in a reasonable amount of time, I implemented importance sampling and the Metropolis-Hastings method. The choice of parameters for the 1D SHO are outlined in Figures 3, 4, and 5.

Through spectral analysis of the transition amplitude and correlation functions, the energy spectrum for the system can be retrieved. The $Z(a,b)$ can rewritten in terms of stationary states $|\phi_n(t)\rangle$ and the corresponding energies E_n defined by the Shrödinger equation:

$$Z(b,a) = \sum_{n=0}^{\infty}\phi_n(x_b)\phi_n^*(x_a)\exp(\frac{-i(E_n - E_0)(t_b - t_a)}{\hbar}). \tag{5}$$

Under Wick rotation, the leading contribution to $Z(b,a)$ is the $(E_1 - E_0)$ decaying exponential. For more complicated transition amplitudes i.e. correlation functions, a similar spectrum decomposition occurs. Correlation functions can be calculated from the Monte Carlo paths via the large time limit of $Z(b,a)$,

$$\langle\phi_0|x(t)x(0)|\phi_0\rangle = \sum_{n=0}^{\infty}|\langle\phi_0|x(0)|\phi_n(0)\rangle|^2\exp(\frac{-E_n\tau}{\hbar}). \tag{6}$$

By using a series of correlation functions with varying energy contributions, the leading energies can be fit and retrieved as shown in Figure 6. The transition from 1D SHO to Lattice QCD begins with the Lagrangian,

$$\mathcal{L}[\psi,\overline{\psi},G] = \sum_{f=1}^{N_f}\overline{\psi}_{a\alpha}^{(f)}(i\gamma_{\alpha\beta}^{\mu}\mathcal{D}_{\mu ab} - m^{(f)}\delta_{\alpha\beta}\delta_{ab})\psi_{a\alpha}^{(f)} - \frac{1}{4}G_{\mu\nu}^a G_a^{\mu\nu}, \tag{7}$$

where $\mathcal{D}_\mu = \partial_\mu + ig\mathcal{A}_\mu$ and $G_{\mu\nu} = -i/g[\mathcal{D}_\mu, \mathcal{D}_\nu]$. ψ and $\overline{\psi}$ are the fermionic quark fields, $\mathcal{A}_\mu$ are the gluon fields, γ^μ are the Dirac gamma matrices, g is the coupling strength, m is the flavor mass, a and b refer to color indices, α and β refer to Dirac indices, μ and ν are the Minkowski spacetime index, and f represents the flavor index. Gluon fields have the SU(3) symmetry dictated by the Gell-Mann matrices and structure constants. The matrix in between the fermionic fields is known as the Dirac matrix. [8]

Though to fully describe QCD, all quark flavors would be included, in our calculation we use "2+1" flavors. The 2 represents the "light" quarks u and d, named due to their light mass (∼3 MeV). In QCD, the charge of the quark does not have any effect and so the only difference between the up and down quarks are their masses. Because their masses are already nearly identical in the energy range of calculation, a degenerate mass m_l is used to describe both and reduces the isospin symmetry to SU(2). The "+1" in "2+1" represents flavor s, the next lightest mass (∼93 MeV) of the quark flavors. The lightest mass quarks have a larger average wavelength, and therefore can be well described with larger lattice spacing where heavier quarks will require finer lattice spacing and much more computational power. The input m_π is often different than the empirically calculated value due to the increased computational intensity. In order to reach the true pion mass, and similarly the continuum limit, many lattice variations are calculated and the continuum limit is extrapolated at the correct pion mass.

The requirement of gauge invariance on the lattice leads to the redefinition of gluon fields to gauge links The fermionic fields are placed on the lattice points and gauge link variables $U_\mu(n) \approx \mathbb{1} + ia\mathcal{A}_\mu(n)$ connect them. Figure 7 shows a graphical representation of this setup. [9] Though there are many other corrections to the discretized action not described here, this is the basic setup across Lattice QCD simulations. When computing the Monte Carlo Markov chains, even with optimal numerical techniques, the largest computational expense is dedicated to inverting the Dirac matrix.

Observables on the lattice are computed in a similar manner as to the 1D SHO example but are integrated over all indices of all fields. Instead of using the position operator as in 1D SHO to compute correlation functions, the two-point correlators used Lattice QCD are constructed from the time-ordered hadronic creation and annihilation operators, $\mathcal{O}(t)$ and $\overline{\mathcal{O}}(t)$ constructed from the quark creation and annihilation operators:

$$C(t) = \langle 0|T\mathcal{O}(t+t_0)\overline{\mathcal{O}}(t_0)|0\rangle. \tag{8}$$

These correlators are grouped together in symmetry channels with similar quantum numbers of momentum $\mathbf{p}$, total spin J, spin projection, parity P, and flavor structure. On a cubic lattice, J is no longer a conserved value and therefore no longer a good quantum number. In its place there are lattice symmetries that form irreducible representation (irreps) that can be used as a quantum number and relate back to the total angular momentum.

Rather than fitting to a series of exponentials there is a more reliable method of retrieving the energies and overlaps onto the ground state. Instead, an important theorem states that the eigenvalues of a correlator matrix have the rough form $b_n\exp(-(E_n - E_0)t)$ [10], a much easier form to fit.

3 Status and Results (∼2)

The results in this writeup are an analysis of the D200 Ensemble computed by the Coordinated Lattice Simulation (CLS) Group. Details on this ensemble can be found in Refs. [11, 12], and a summary of the important input parameters are given in Table 1. The CLS Group generated the field configurations using JUQUEEN [13], and Dr. Colin Morningstar's group calculated the correlation functions from the configurations on Frontera [14].

I am currently contributing to an analysis of $N\pi$ scattering with total isospins $I = 1/2$ and $I = 3/2$. The final results on the report will include the energy spectrum and phase shift calculations, though only the energy spectrum will be shown here.

To reduce autocorrelation, the CLS Group only used every τ_{meas} configurations in the Monte Carlo-Metropolis Hastings chain (similar to N_{sweeps}) in the SHO example). To gauge the effects of autocorrelation in our results, we used the bootstrap calculated error bar from the correlators. If there the autocorrelation effects are negligible, then the error bars should not change when the samples are rebinned. Autocorrelation effects lead to an underestimation of the errors which was observed in the initial analysis of the $N\pi$ channels of D200 (Figure 8). To account for this, we rebinned every 20 samples where the error bars begin to converge.

Before we can calculate the spectrum for an interacting system, first we fit to the non-interacting correlators (correlators that contained only N or π) as shown in Figure 9. To gain confidence in the fits, we fitted to multiple fit forms on a series of ranges and compared the results in Figure 10. The value determined is stable across fit forms and several t_{min} choices.

The full spectrum calculated for all irreps is shown in Figures 11 and 12. The fit results of the energies are in lattice units and therefore to see meaningful results we use units of m_π. These units can be obtained by simply dividing the pion rest mass fit from every value. To get a sense of how the Roper resonance affects the levels, we compare the interacting system to constructions of the non-interacting levels of N and π. Interacting system energy levels significantly shifted from the non-interacting levels can be seen in the isoquartet channel irreps $H_g(0)$, $G2(1)$, $F1(3)$, $F2(3)$, $G(3)$, $G1(4)$, and $G2(4)$. The isodoublet channel does not feature significantly shifted energies (within the $N\pi$ and $N\pi\pi$ thresholds).

4 Conclusions and Next Steps (∼1)

Based on these results, we concluded that the isodoublet channel of the $N\pi$ interactions is a weakly interacting channel due to its alignment with the non-interacting energy levels (within these threshholds). On the other hand, the isoquartet channel shows sign of the Δ resonance. Using these level calculations, my collaborators, John Bulava and Fernando Romero-Lopez, are calculating the phase-shifts and other important scattering observables from the spectrum [15]. At the current moment, the precision that we have reached for these phase shifts has not been achieved before. My collaborators can also show how the Δ resonance appears and affects the phase shift calculation. With upcoming results, I can learn more about the Δ resonance and how it affects observables.

Thanks to the efforts of the CLS group the $N\pi$ channel is one of many channels calculated from the D200 ensemble. There are NN channels to analyze, $Llambda\Lambda$, and so on. There is plenty of data in need of investigation in a similar manner as the $N-\pi$ channels. I am personally excited to investigate interactions with strange quarks. I hope by studying these channels and Lattice QCD, I can use this knowledge to investigate constructing three-point correlators and "quark currents" [16] to calculate more complicated observables such as the N axial form factor and the $N-\Delta$ transition form factor, information needed for the DUNE experiment.

5 Basic Physics Connections (∼1)

To connect this work to basic physics, I would like to discuss how the action relates to both quantum mechanics and classical mechanics and why Monte Carlo importance sampling is a great tool for simulating quantum mechanics. To begin, I will return to the 1D SHO example and rewrite the SHO Action,

$$S = \int_{t_a}^{t_b} dt \left(\frac{1}{2} m \dot{x}^2 + \frac{1}{2} m \omega^2 x^2 \right). \tag{9}$$

The action is related to classical mechanics via the principle of least action that states for a small change in x, the change in the action, δS, is zero. This requirement captures classical mechanics because the result is that the path of x is deterministic. When the principle of least action is required, it determines the equation of motion. For the SHO, the equation of motion is

$$\ddot{x}_{\text{cl}} + \omega^2 x_{\text{cl}} = 0. \tag{10}$$

If you know the initial velocity and position of the particle, then the equation of motion maps out where the particle will be at any give time in the future. This is shown in Figure 1, where x_{cl} represents the classical path through time. Quantum mechanics, however, is not so deterministic, though it does have predictable characteristics. Rather than the set path, x_{cl}, the quantum path from (t_a, x_a) to (t_b, x_b) can be defined as $x = x_{\text{cl}} + \chi$ where the only limitations to $\chi(t)$ is $\chi(t_a) = \chi(t_b) = 0$. Though under quantum mechanical paths can take any path, there are some limitations. There are definite probabilities and average distributions of particles, indicating that their randomness is reigned in. These probabilities are well defined by the Schrödinger equation in the nonrelativistic limit. By using the transition amplitude in our Monte

Carlo importance sampling, we are imposing the Schrödinger equation determined probability functions upon the randomly generated configurations.

References

[1] *2021: particle listings*, https://pdg.lbl.gov/2021/listings/contents_listings.html.

[2] D. J. Gross and F. Wilczek, "Ultraviolet behavior of non-abelian gauge theories", Phys. Rev. Lett. **30**, 1343–1346 (1973).

[3] H. D. Politzer, "Reliable perturbative results for strong interactions?", Phys. Rev. Lett. **30**, 1346–1349 (1973).

[4] W. A. Bardeen and C. T. Hill, "Chiral dynamics and heavy quark symmetry in a solvable toy field-theoretic model", Phys. Rev. D **49**, 409–425 (1994).

[5] "Long-baseline neutrino facility (lbnf) and deep underground neutrino experiment (dune) conceptual design report, volume 2: the physics program for dune at lbnf", 10.2172/1264020 (2015).

[6] *Home*, https://www.dunescience.org/.

[7] S. Skinner, *Mcmhmc-1d-sho*, https://github.com/xinucode/MCMHMC-1D-SHO/blob/main/SHOexample.ipynb.

[8] *Quantum chromodynamics - particle data group - 2020 review*, (Aug. 2019) https://pdg.lbl.gov/2020/reviews/rpp2020-rev-qcd.pdf.

[9] C. Gattringer and L. B. Lang, *Quantum chromodynamics on the lattice* (Springer-Verlag).

[10] M. Lüscher and U. Wolff, "How to calculate the elastic scattering matrix in two-dimensional quantum field theories by numerical simulation", Nuclear Physics B **339**, 222–252 (1990).

[11] M. Bruno et al., "Simulation of QCD with $N_f = 2 + 1$ flavors of non-perturbatively improved Wilson fermions", JHEP **02**, 043 (2015).

[12] G. S. Bali, E. E. Scholz, J. Simeth, and W. Söldner (RQCD), "Lattice simulations with $N_f = 2 + 1$ improved Wilson fermions at a fixed strange quark mass", Phys. Rev. **D94**, 074501 (2016).

[13] *Juqueen*, https://web.archive.org/web/20190118115058/https://www.fz-juelich.de/ias/jsc/EN/Expertise/Supercomputers/JUQUEEN/JUQUEEN_node.html.

[14] *Texas advanced computing center*, https://www.tacc.utexas.edu/systems/frontera.

[15] M. Lüscher, "Two particle states on a torus and their relation to the scattering matrix", Nucl. Phys. **B354**, 531–578 (1991).

[16] C. J. Shultz, J. J. Dudek, and R. G. Edwards, "Excited meson radiative transitions from lattice qcd using variationally optimized operators", 10.48550/ARXIV.1501.07457 (2015).

6 Tables and Figures

β	a[fm]	$L^3 \times T$	m_π, m_K[MeV]	τmeas[MDU]	N_{conf}
3.55	0.064	$64^3 \times 128$	200,480	8	2000

Table 1: Parameters of the D200 ensemble produced by the CLS. The first column (β) is the lattice gauge coupling defined in Ref. [12], which is followed by the spatial lattice spacing, the pseudoscalar meson masses, the separation between correlation function measurements and molecular dynamics units (MDU), and the number of gauge configurations measured.

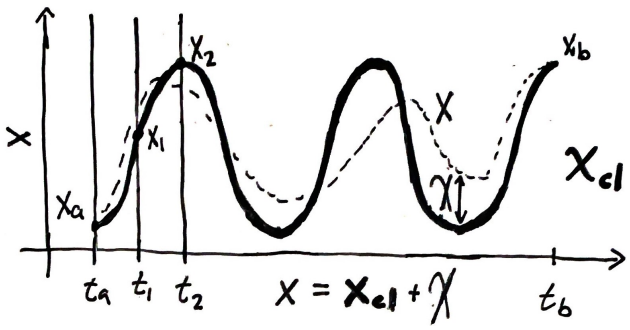

Figure 1: A sketch of the nonzero velocity classical path, x_{cl} of the one-dimensional (1D) simple harmonic oscillator (SHO) on a 1D lattice. The time domain $[t_a, t_b]$ is discretized to N elements with spacing ε between each time index. x indicates the position of the particle. χ represents the difference between the classical path and a quantum path from (t_a, x_a) to (t_b, x_b).

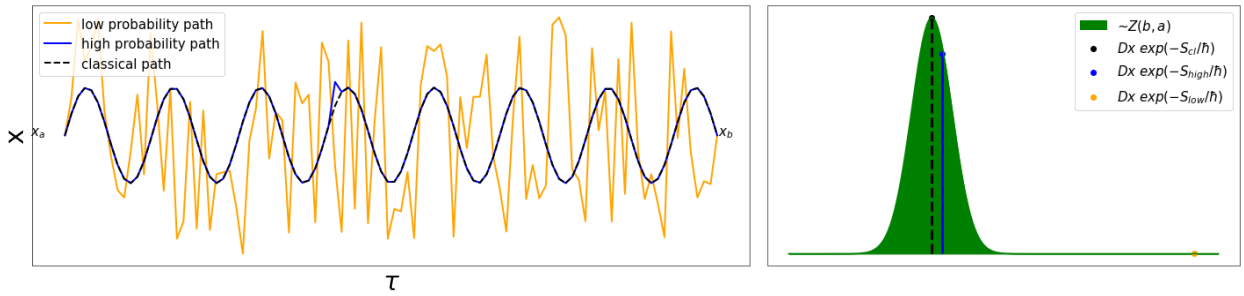

Figure 2: Two figures generated from script created by the author available at [7]. Left: several possible paths of the 1D SHO in Euclidean time (Wick rotated time domain). Right: Each path's corresponding contribution to the total transition amplitude. S_{cl} is computed from the classical path, S_{high} is computed from the high probability path, and S_{low} is computed from the low probability path.

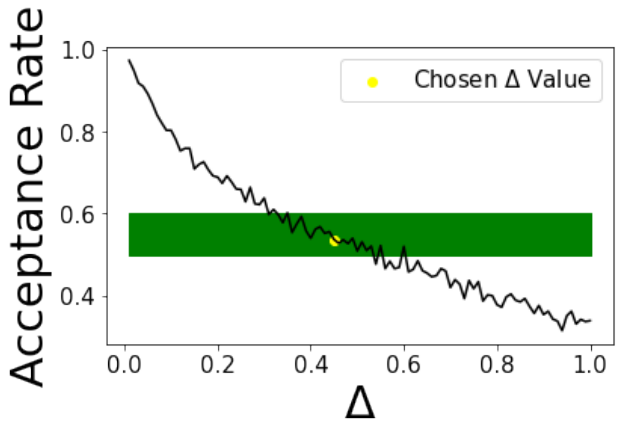

Figure 3: Monte Carlo importance sampling acceptance rate versus maximum magnitude of δx update. In the MCMHMC SHO Example repository available at Ref. [7], the rudimentary simulation performs a series of updates to a given lattice configuration. The chosen parameter $\Delta = 0.45$ is in yellow, and the target range is highlighted in green. At each point on the lattice, it suggests an update by selecting a random number in the range $[-\Delta, \Delta]$. The update is then accepted or rejected based on the change in the action. For an optimized yet accurate MCMHMC program, the should be somewhere within this target range.

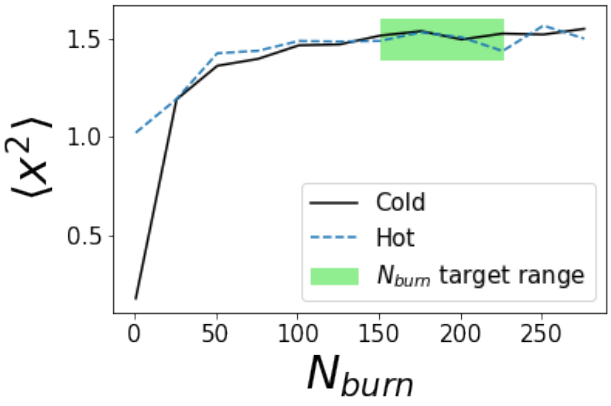

Figure 4: Average x^2 versus number of "burn" sweeps. In the MCMHMC SHO Example repository available at Ref. [7], the rudimentary simulation performs a series of updates to a given lattice configuration. To initialize the lattice, there is a "hot" and "cold" configuration. The hot configuration is setting every element to a random number within Δ. The cold configuration is where every position at every time is set to zero. Neither of these configurations reflect the quantum mechanical behavior well, and therefore we perform N_{burn} sweeps on the lattice to and see when an observable "thermalizes". The N_{burn} chosen in this simulation was 200.

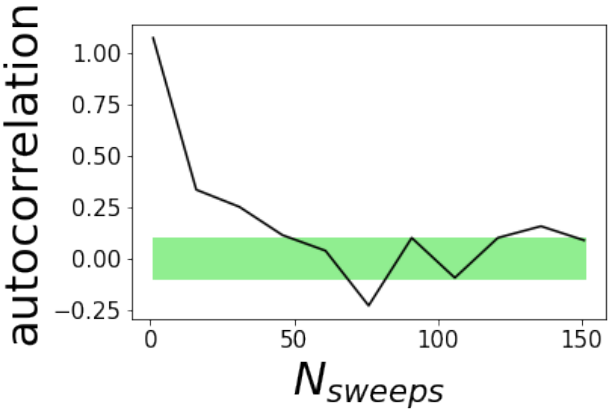

Figure 5: Autocorrelation between measurements versus number of sweeps N_{sweeps} between each measurement. Data from the MCMHMC SHO Example repository available at Ref. [7]. Target range for negligible autocorrelation is less than 0.1. The chosen number of sweeps to perform each measurement was 120.

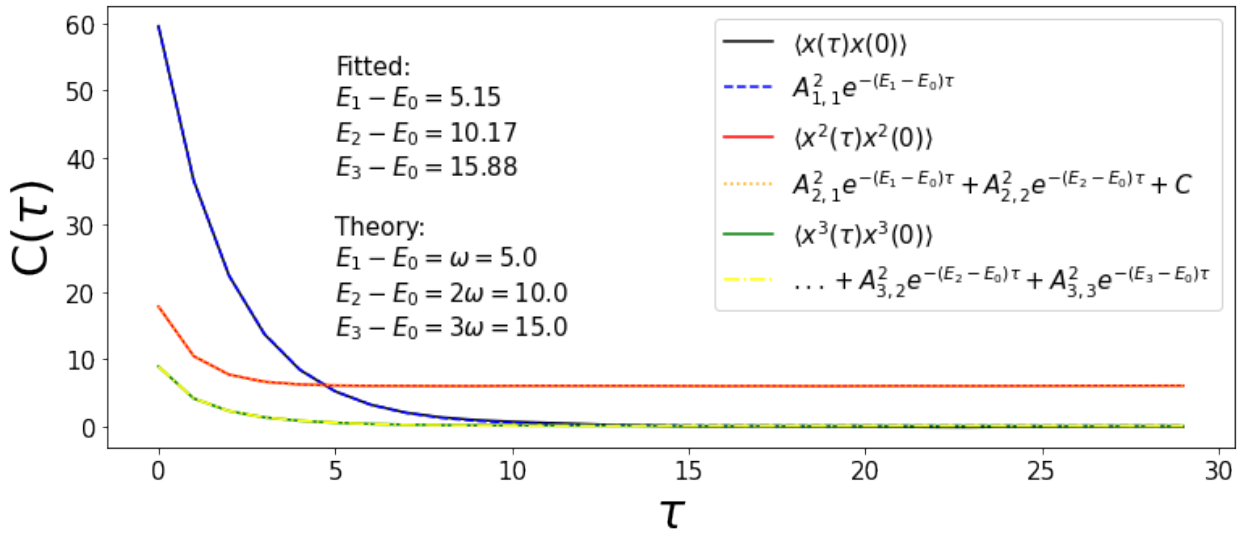

Figure 6: Several fitted correlation functions produced from MCMHMC SHO Example repository available at Ref. [7]. The fit results are compared to analytical calculations.

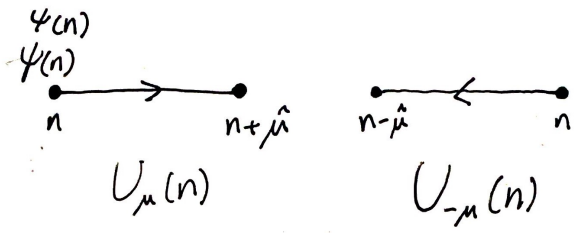

Figure 7: Graphical representation of gauge link variables. See Figure 2.2 of Ref [9].

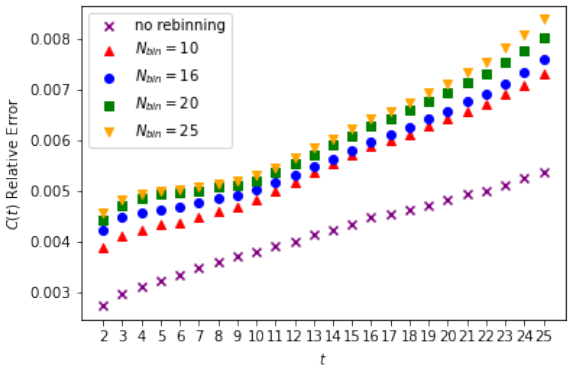

Figure 8: Pion correlator error of the single hadron pion with momentum of zero. Relative correlator errors of rebinned measurements were calculated using bootstrap sampling with $N_{\mathrm{B}} = 2000$. Original errors and error calculated from N_{bin} with values 4, 8, 10, and 16 are shown here to emphasize the convergence of the errors. We were limited by the choice of N_{bin} due to the fact that they were required to be factors of $N_{\mathrm{conf}} = 2000$.

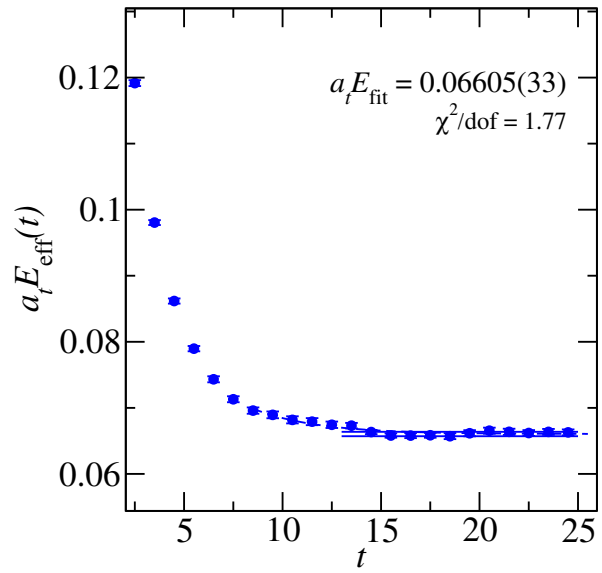

Figure 9: Effective mass versus lattice time calculated of the momentum zero pion correlator from the D200 ensemble. Effective mass is calculated from the correlator by the relation $\ln(C(t)/C(t+1))$. Viewing the effective mass gives a sense of the higher energy contamination is affecting the correlator. For a single exponential fit, the range of the fit is limited to the plateau of this plot. Other fit forms to account for the higher energy contamination are also analyzed.

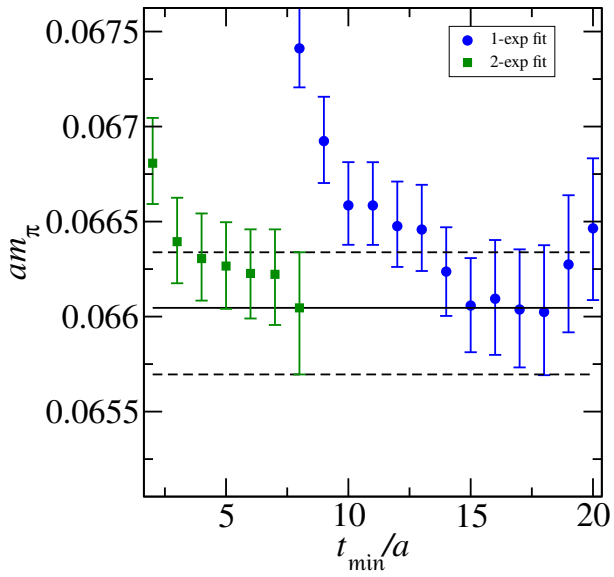

Figure 10: $t_{\rm min}$-plots for the determination of am_π (left) and am_N. Both single- and two-exponential fits are shown, and the horizontal band indicates the chosen value. The consistency between single- and two-exponential fits is reassuring.

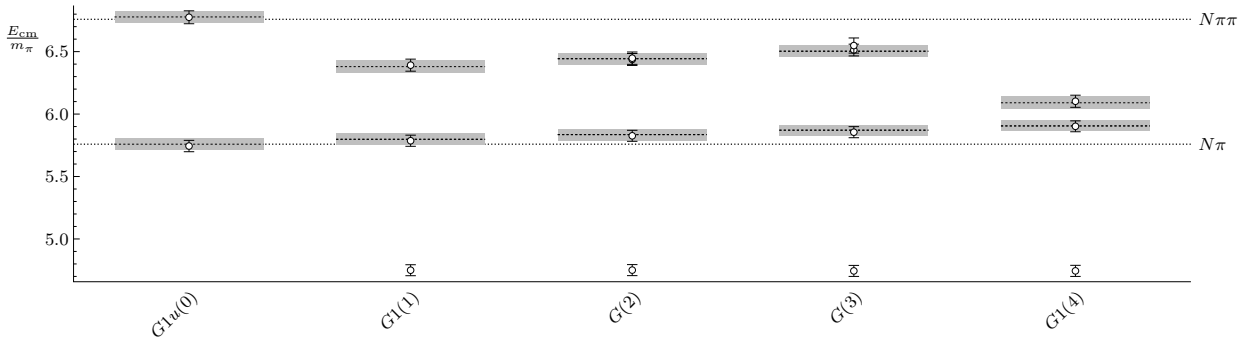

Figure 11: $N\pi$ isodoublet channel spectrum calculated on the D200 ensemble. The notation along the horizontal axis is $\Lambda(\mathbf{P}^2)$, where $\mathbf{P}^2$ is the total momentum squared and Λ is the irrep of little group $\mathbf{P}$. Dashed lines indicate the limits of the elastic region. Solid lines and shaded regions indicate the non-interacting $N\pi$ levels and their error bars.

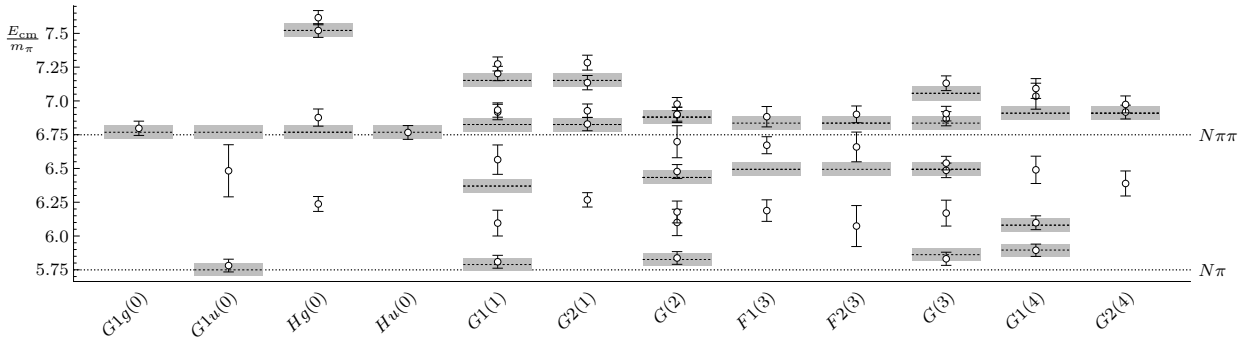

Figure 12: $N\pi$ isoquartet channel spectrum calculated on the D200 ensemble. The notation along the horizontal axis is $\Lambda(\mathbf{P}^2)$, where $\mathbf{P}^2$ is the total momentum squared and Λ is the irrep of little group $\mathbf{P}$. Dashed lines indicate the limits of the elastic region. Solid lines and shaded regions indicate the non-interacting $N\pi$ levels and their error bars.